Moisture transport from the Atlantic to the Pacific basin and its response to North Atlantic cooling and global warming

INGO RICHTER*

International Pacific Research Center, University of Hawaii at Manoa, Honolulu, Hawaii

SHANG-PING XIE

International Pacific Research Center and Department of Meteorology, University of Hawaii at Manoa, Honolulu, Hawaii

submitted to

Climate Dynamics

accepted, November 10, 2009

Corresponding author:

Ingo Richter

* Current affiliation:

Research Institute for Global Change, JAMSTEC, Yokohama, Japan

E-mail: richter@jamstec.go.jp

ABSTRACT

Atmospheric moisture transport from the Atlantic to the Pacific basin plays an important role in regulating North Atlantic salinity and thus the strength of the thermohaline circulation. Potential changes in the strength of this moisture transport are investigated for two different climate-change scenarios: North Atlantic cooling representative of Heinrich events, and increased greenhouse gas (GHG) forcing. The effect of North Atlantic cooling is studied using a coupled regional model with comparatively high resolution that successfully simulates Central American gap winds and other important aspects of the region. Cooler North Atlantic sea surface temperature (SST) in this model leads to a regional decrease of atmospheric moisture but also to an increase in wind speed across Central America via an anomalous pressure gradient. The latter effect dominates, resulting in a 0.13 Sv (1 Sv = 10^6 m^3 s^{-1}) increase in overall moisture transport to the Pacific basin. In fresh water forcing simulations with four different general circulation models, the wind speed effect is also present but not strong enough to completely offset the effect of moisture decrease except in one model. The influence of GHG forcing is studied using simulations from the Intergovernmental Panel on Climate Change archive. In these simulations atmospheric moisture increases globally, resulting in an increase of moisture transport by 0.25 Sv from the Atlantic to Pacific. Thus, in both scenarios, moisture transport changes act to stabilize the thermohaline circulation. The notion that the Andes effectively block moisture transport from the Atlantic to the Pacific basin is not supported by the simulations and atmospheric reanalyses examined here. This indicates that such a blocking effect does not exist or else that higher resolution is needed to adequately represent the steep orography of the Andes.

1 Introduction

The narrow Central American isthmus with its comparatively low orography (Fig. 1) affords substantial transport of atmospheric moisture from the Atlantic to the Pacific basin by the northeasterly trades. This freshwater export leads to salinification of subtropical Atlantic waters, which are subsequently carried by the prevailing currents to high latitudes, where they cool and sink. In this way the Atlantic moisture export forms a crucial element in North Atlantic deep water formation and the thermohaline circulation (THC; Zaucker and Broecker 1992; Romanova et al. 2004), which are vital components of the global climate system (Broecker 1997; Clark et al. 2002). The strength of the inter-basin transport may thus provide an important feedback mechanism that either amplifies or damps anomalies in the thermohaline circulation. THC weakening is thought to have occurred seven times over the last 60 ka (1 ka = 1000 years; e.g. Hemming 2004) but also features in many projections of future climate change under greenhouse gas (GHG) forcing (Stouffer and Manabe 1999; Gregory et al. 2005; Swingedouw et al. 2007). It is therefore of interest to examine how inter-basin transport responds under these two forcing scenarios.

Past periods of drastic changes in the THC were associated with freshwater discharge into the North Atlantic, which disrupted deep water formation and led to a shutdown of the Atlantic meridional overturning circulation (AMOC), the Atlantic branch of the THC. These periods are the Heinrich events and the Younger Dryas (e.g. Broecker 2003). The former are believed to have been the result of catastrophic iceberg discharges from the Laurentide ice sheet (e.g. Hemming 2004), and are documented by ice-rafted detritus that was eventually deposited on the ocean floor. The North Atlantic sea-surface temperature (SST) cooling associated with these events also affected the subtropical oceans (as evidenced by sediment cores [e.g. Leduc et al. 2007; Pahnke et al. 2007]) and led to a southward shift of the Atlantic intertropical convergence zone (ITCZ). How such conditions would influence the inter-basin moisture transport is a matter of current debate. One line of argument concludes that transport should decrease since the atmospheric moisture content east of Central America decreases as the ITCZ shifts southward (Zheng et al. 2000; Benway et al. 2006; Leduc et al. 2007), leading to a decreased moisture flux across the isthmus. This argument, however, fails to take into account the effect of cold North Atlantic SSTs on atmospheric winds. Considering this impact one finds that winds across Central America might increase because the cold SSTs induce an inter-basin pressure gradient that increases the northeast trades. This in turn would increase atmospheric moisture export. Which of these two effects is dominant is still under debate. In terms of proxy records, there is support for both increased (Pahnke et al. 2007) and decreased (Leduc et al. 2007) moisture transport. A study with a general circulation model (GCM), on the other hand, finds that moisture transport across the American continent increases by 0.1 Sv (1 Sv = 10^6 m^3 s^{-1}) when an anomalous freshwater flux is applied to the North Atlantic (Lohmann, 2003). The model used by Lohmann (2003) , however, employed a rather coarse resolution (T21 or 5.6° in the horizontal) and experienced some problems in simulating the atmospheric flow over the Central American isthmus during summer. Similar results were also found by Lohmann and Lorenz (2000) in an atmospheric GCM with prescribed SST representing the conditions during the last glacial maximum (LGM). Relative to present day conditions, the LGM featured cooling of the tropical SST that was more pronounced on the Atlantic than the Pacific side.

The above discussion on the impact of an ITCZ shift on Atlantic moisture export implicitly assumes that the Andes effectively block any transport, so that the bulk of the moisture is channeled across the Central American Isthmus. This appears to be a reasonable assumption as the Andes rise above 2000 m at almost all latitudes (Fig. 1) and atmospheric moisture content decreases rapidly with height. Whether it holds true in the context of large-scale models and to what extent model resolution and orographic heights might play a role, is a question that we will address in the present study.

Moisture export from the Atlantic basin has also received a lot of attention in the context of global warming studies (Manabe and Stouffer 1988; Schiller et al. 1997; Latif et al. 2000; Swingedouw et al. 2007) because it might play a crucial role in the stabilization of the thermohaline circulation in a warming climate. GCMs typically predict a weakening of the AMOC under greenhouse gas forcing. This is due to increased surface net energy and freshwater flux into the North Atlantic Ocean and, to a lesser extent, increased poleward atmospheric moisture flux (Gregory et al. 2005). Under strong CO_2 forcing, such as quadrupling CO_2, these effects can lead to a complete shutdown of the thermohaline circulation with drastic consequences for the North Atlantic region (Manabe and Stouffer 1994; Chan and Motoi 2005). Moisture export across the Central American isthmus could therefore be an important factor opposing the slowdown of the AMOC and perhaps even preventing its collapse (Latif et al., 2000; Swingedouw et al., 2007).

The above considerations illustrate that moisture export from the Atlantic plays an important role in both paleoclimate and global warming contexts. It is therefore highly desirable to obtain realistic estimates of this quantity from model simulations as well as observations. All of the modeling studies cited above use GCMs with resolutions of 2.5° or coarser and can therefore not resolve adequately the detailed orography of the Central American isthmus. In the present study we therefore use a regional atmospheric model with comparatively high resolution to investigate the impact of Atlantic SSTs on the moisture transport across Central America. With its grid size of 0.5° x 0.5° the model is able to produce a realistic simulation of the eastern Pacific and western Atlantic regions and, in particular, of the Central American gap winds. The goals of our study are twofold: 1) Re-examine the effect of North Atlantic cooling on moisture export in the context of a regional model than can resolve Central American orography and that realistically simulates cross-isthmus winds. 2) Analyze the role of moisture export in global warming scenarios using state-of-the-art climate models.

The regional model and experimental set up are introduced in section 2. Section 3 discusses Atlantic-to-Pacific moisture transport under current climate as simulated in various models, and shows that there is an overlooked yet substantial transport across the northern Andes. Experiments with this model, which we present in section 4, suggest that during North Atlantic cooling the effect of the enhanced northeast trades dominates over the reduced atmospheric moisture content. In section 5 we analyze moisture export from the Atlantic basin in GCM simulations under both present day and CO_2 doubling forcing scenarios and compare these to earlier results. We discuss our results in section 6.

2 Model and experiments

The model used in this study is a regional ocean-atmosphere model (ROAM) developed at the International Pacific Research Center (IPRC), University of Hawaii, in collaboration with the Frontier Research Center for Global Change (FRCGC) in Japan (hereafter we refer to this model as IROAM). The atmospheric component is a finite-difference model with full physics (Wang et al. 2004). The model's resolution is 0.5° x 0.5° in the horizontal and 28 sigma levels in the vertical. The model physics include a convection scheme based on Tiedtke (1989), longwave and shortwave parameterizations (Edwards and Slingo 1996; with improvements by Sun and Rikus 1999), cloud microphysics (Wang 2001), a non-local closure scheme for vertical turbulent mixing (Langland and Liou 1996), and a land surface model (Dickinson et al. 1993). A more detailed description of the model can be found in Wang et al. (2003). The oceanic component is the Geophysical Fluids Dynamics Laboratory (GFDL) MOM 2 (Pacanowski 1996). The configuration used here has the same horizontal grid as the atmospheric model and 35 vertical levels. The oceanic and atmospheric model domains are as follows. The oceanic component covers the Pacific basin from coast to coast between 35°S and 35°N. The atmospheric model domain covers the area 150°W – 30°W, 35°S – 35°N, which includes the eastern tropical Pacific and the tropical American continent. At the open boundaries, the atmospheric model is restored to the four times daily reanalysis of the National Centers for Environmental Prediction (NCEP) and National Center for Atmospheric Research (NCAR; Kalnay et al. 1996). The ocean model uses monthly Levitus (1982) climatology at its boundaries. The coupling strategy is as follows. West of 150°W the ocean surface is forced with the NCEP/NCAR reanalysis. Between 150°W and the American coast ocean and atmosphere are fully coupled. In the Atlantic part of the domain, the atmospheric model is forced with monthly mean observed SST.

Two experiments are used to analyze the moisture transport across Central America and its sensitivity to Atlantic conditions. The control experiment (CTRL hereafter) uses the observed SSTs outside the coupling domain as stated in the model description. The second experiment (NAC hereafter) simulates a North Atlantic cooling event by prescribing a 2 K cold anomaly in the Atlantic north of 5°N. The anomaly is tapered off between 5°N and 5°S. This pattern of cooling is similar to the ones simulated in Atlantic "water-hosing" GCM experiments, in which anomalous fresh water flux is applied to the North Atlantic. While less realistic than an actual water-hosing scenario, the setup is well-suited to examine the qualitative response of the Atlantic moisture export to North Atlantic cooling. Here our focus is on the influence of North Atlantic cooling on inter-basin moisture transport. The attendant circulation changes are analyzed in more detail by Xie et al. (2008). A concern with the NAC experiment is, whether the present day boundary forcing overly constrains the model circulation in the interior. However, sensitivity tests with IROAM have shown that the interior dynamics can change significantly between experiments even when the lateral boundary forcing remains the same (Xie et al. 2007). Removing cloud feedbacks south of the equator, for example, led the model to develop a double ITCZ, illustrating the degree to which interior dynamics can change under unchanged boundary forcing.

Both CTRL and NAC were integrated for 8 years using boundary forcing for the period 1996-2003. Since in NAC the model takes about 1-2 years to equilibrate the last 6 years of each integration were used for analysis. CTRL produces a realistic simulation of the tropical Pacific including the seasonal evolution of the ITCZ, the Peruvian stratocumulus decks, and the equatorial cold tongue (see Xie et al. 2007 for a more detailed description of the model's performance in the eastern tropical Pacific). The model also successfully reproduces the low-level wind field across the Central American isthmus. The orography of this isthmus is marked by three elevation gaps (Fig. 2a) which afford strong low-level winds during boreal winter. These gaps are approximately located at the Gulfs of Tehuantepec, Papagayo, and Panama and the strong wintertime jets that emerge from them are named accordingly. All three of these jets are reproduced in the model and compare favorably with QuickSCAT observations (Fig. 2b). They are, however, somewhat weaker than observed, especially the Panama jet, which also does not extend as far south as in QuickSCAT. This is likely due to the model not fully resolving the elevation gaps of the Central American orography. An atmosphere-only version of IROAM run at 0.25° x 0.25° produces a Panama jet that is stronger but still positioned too far north (Xu et al. 2005). Overall, however, IROAM produces rather realistic winds across Central America, which lends credence to the results of our moisture transport calculations.

For the analysis of moisture transport under global warming we use simulations from the Fourth Assessment Report (AR4) of the Intergovernmental Panel on Climate Change (IPCC), performed using the Special Reports on Emission Scenarios (SRES) A1B scenario. In these simulations, CO_2 concentrations increase from 2000-2100 and remain constant afterward. Resolution varies considerably across models (see Table 1) from 1.125° lon by 1.125° lat (T106) and 56 vertical levels in the MIROC high resolution model, to 5° lon by 4° lat and 20 levels in the GISS EH and ER models, which allows us to explore resolution dependence. As a reference, we also calculated moisture transport for the European Centre for Medium-Range Weather Forecasts (ECMWF) 40-year global ReAnalysis (ERA 40; Uppala et al. 2005; http://www.ecmwf.int/research/era/), and the Japanese 25-year Reanalysis Project (JRA-25; Onogi et al. 2007; http://jra.kishou.go.jp/index_en.html).

To calculate moisture transport across the Americas we define thirteen line segments that approximately run along the Atlantic drainage divide (Fig. 1). Integrating the moisture flux across each line segment we obtain the cross-isthmus moisture transport. The equation for an individual line segment is

$$tr = \int_p \int_l uq\,dl\,\frac{dp}{g} \tag{1}$$

where *tr* is the moisture transport across the line segment, *p* is pressure, *l* is position along the segment, *u* is velocity normal to the segment, *q* is specific humidity and *g* is the gravitational constant. We decompose the moisture flux, *uq*, in NAC into the following components:

$$uq = \overline{u}\overline{q} + u'\overline{q} + \overline{u}q' + u'q' \tag{2}$$

where the overbar denotes CTRL and the prime denotes the difference NAC minus CTRL, i.e., $u' = u - \overline{u}$. This decomposition allows us to separate the effects of moisture and windspeed changes. The procedure for calculating the moisture transport is similar to the one used in Xu et al. (2005) but in addition to the vertical integral also outputs the vertical structure of the transport. Transports are calculated based on daily means. Using monthly means, however, only decreases values by about 0.2%. This suggests that transients do not play an important role, which is to be expected in the subtropics.

3 Moisture export under current climate conditions

Moisture transport across the tropical Americas (segments 5-12 in Fig. 1) under current climate conditions is listed in Table 2 and plotted as a bar chart in Fig. 3. Transport ranges from 0.29 Sv in the UKMO to 0.72 Sv in the CSIRO model. The ensemble mean transport is 0.56 Sv and thus fairly similar to the 0.54 Sv simulated by IROAM. The reanalyses occupy the lower end of the spectrum with 0.34 Sv in ERA 40 and 0.40 Sv in JRA 25, which compares well with the 0.36 Sv from the observational estimate by Zaucker and Broecker (1992). This might indicate a tendency in the AR4 models and IROAM to overestimate the transport across the tropical Americas. An estimate based on NCEP reanalysis (Zhou et al., 2000), on the other hand, amounts to 1.05 Sv and thus exceeds even the highest estimate of the models surveyed here. Clearly, there is a need to further constrain the plausible range of cross-American moisture transport. However, our own transport calculations for the ERA 40 and JRA 25 reanalyses agree rather well.

Horizontal model resolution and magnitude of simulated transport do not appear to be correlated significantly. For example, while resolution is similar in the CSIRO and UKMO models, they lie at opposite ends of the scale in terms of transport. It should be noted, however, that the only two models that solely differ in resolution (the two MIROC models), produce significantly different transports, with 0.51 and 0.71 Sv in the high and medium resolution versions, respectively.

Figure 4 shows vertical cross sections of annual mean specific humidity and velocity for the tropical Americas (segments 3-13 in Fig. 1). Wind velocity is defined normal to the line segments, with a positive sign denoting flow toward the Pacific side. The cross-basin moisture transport is accomplished by three jets over Tehuantepec (segment 6), Papagayo (8), and the northern Andes (11). The Panama jet is a winter-to-early-spring phenomenon (Xie et al., 2005) and does not contribute much to the annual-mean flux. A noteworthy feature in Fig. 4 is the substantial transport across the northern Andes because it contradicts the notion that the Andes pose a barrier to moisture transport (e.g. Leduc et al. 2007). In many models, transport across the Andes actually exceeds that across Central America. Only the ERA 40 reanalysis shows little transport across the Andes, which is mostly due to the low wind speed (especially over the northern Andres, segment 11), rather than moisture anomalies (Fig. 5). It is also apparent that atmospheric moisture content is still considerable even at the height of the model-resolved Andes. Its values are around 18 g/kg at the sea level and 10 g/kg over the northern Andes (segment 11) at 800 hPa.

4 Response to North Atlantic cooling

4.1 Annual mean

The influence of North Atlantic cooling on the lower troposphere is summarized in Fig. 6, which shows changes in precipitable water and wind (NAC minus CTRL). Precipitable water decreases over the North Atlantic, consistent with the cooling effect of the prescribed SST anomaly. While the prescribed SST anomaly is spatially uniform, the decrease in precipitable water is most pronounced over the Caribbean. It is apparent that the negative anomaly in precipitable water is advected across Central America to the Pacific side, as the decrease extends much farther downstream toward the western edge of the domain. Figure 6 also features an anomalous anticyclonic circulation centered on the Caribbean. The southern flank of this circulation strengthens cross-isthmus flow and therefore increases the cross-isthmus moisture transport. Figure 6 thus indicates the competing effects of moisture and wind changes on cross-isthmus transport. For a quantitative assessment of the two effects we turn to the transport calculations described in section 2.

In CTRL, the total time-averaged moisture transport across the tropical Americas (segments 5-12 in Fig. 1) amounts to 0.54 Sv. In NAC the transport is 0.61 Sv, an increase of roughly 13%. The 6-year simulation period is too short to allow meaningful significance tests of this increase. We note, however, that the transport in NAC consistently exceeds that in CTRL in every simulation year. The change in transport is largely due to the intensification of the Papagayo and Panama gap winds (Fig. 7b). The Tehuantepec gap winds, on the other hand, decreases by about 1 m/s as do the winds further northwest.

The competing effects of moisture and windspeed changes are illustrated by Fig. 8, which shows the annual mean vertical profile of moisture transport across the segments. The dashed green line in this figure represents the response one would obtain considering moisture changes only, as done, e.g., by Leduc et al. (2007). The result is a decrease of transport throughout the tropospheric column that amounts to 0.08 Sv. This, however, is opposed by the effect of the increase in cross-isthmus windspeed (blue dotted line in Fig. 8), which totals 0.15 Sv. In the lower troposphere below 600 hPa the wind speed effect dominates, resulting in increased moisture transport to the Pacific basin. Above 600 hPa, on the other hand, moisture transport decreases, which is consistent with the fact that wind speed differences are small or negative there while specific humidity is still decreased as seen in Fig. 7. Due to the high moisture content at low levels the overall moisture transport increases by 0.07 Sv or 13% relative to CTRL.

We next analyze how the increased moisture export affects precipitation and evaporation west of Central America. Several sediment cores from this region have been used to deduce sea surface salinity (SSS) changes over the past 100 ka (Leduc et al. 2007; Pahnke et al. 2007). The records thus obtained are often regarded as representative of Atlantic moisture export (Leduc et al. 2007). The implicit assumption is that the moisture transport increase will result in an increase in precipitation and a decrease in surface salinity in the far eastern North Pacific, but the relation might not be that simple. It is therefore of interest to examine how the increased moisture transport in our simulation might affect salinity in the eastern Pacific.

Figure 9 shows precipitation, evaporation and the difference, precipitation minus evaporation (P-E), for CTRL and CTRL minus NAC. Over the Caribbean, precipitation (Fig. 9d) and evaporation (Fig. 9e) both decrease in NAC, consistent with a weakening of the hydrological cycle that is to be expected from the cold SST anomaly. Precipitation also decreases on the Pacific side, off the coast of Central America, and increases further west and to the south. This is consistent with the decrease of precipitable water southwest of Central America shown in Fig. 6. Thus the additional moisture from the Atlantic does not immediately precipitate after crossing the isthmus and does not directly affect the salinity balance in the far eastern tropical Pacific. Evaporation, on the other hand, increases on the Pacific side. This is consistent with the enhanced windspeed in NAC and the effect of the cold Atlantic air encountering warmer surface temperatures after crossing Central America. The precipitation minus evaporation difference (Fig. 9f) shows negative values on both sides of the isthmus, and thus the overall balance shifts toward more evaporation and salinification in NAC. Farther west, however, between 8°N and 20°N, the precipitation increase dominates and freshens the Pacific. These changes are consistent with the SST cooling and southward shift of the Pacific ITCZ that results from the enhanced surface winds.

4.2 Seasonal response

This section takes a closer look at the seasonal variations of moisture transport across the Central American isthmus (segments 5-10). Proxy records often reflect a particular season associated with biological activity or rainfall patterns. Stalagmite records in Central America, for example, typically reflect the summer season because of the monsoon rains.

Substantial seasonal variability is shown in the seasonal time-height sections of moisture transport (Fig. 11). Relative to CTRL the moisture transport in NAC increases between May and December with the maximum change in September. From January to April, on the other hand, there is a slight decrease in moisture transport. These seasonal changes are mostly confined to the lower troposphere. Above 750 hPa transport is lower in NAC than in CTRL throughout the year in accordance with the decreased atmospheric moisture content on the Atlantic side.

The P-E difference is also subject to seasonal changes (Fig. 12), which are dominated by precipitation changes. During DJF differences are moderate and indicate a slight northward shift of the Pacific ITCZ in NAC. The anomalies are organized in a north-south pattern, with P-E decreased in a zonal band between the equator and 8°N, and increased elsewhere. During JJA the P-E changes are more pronounced with decreases as low as 12 mm/day over the coastal waters on both sides of the isthmus. While more intense, the P-E deficit is also more confined to the coastal region and accompanied by a P-E increase to the southwest resulting in a northwest oriented dipole pattern. This more pronounced response in JJA is likely due to the fact that winds in NAC do not converge over Central America as they do in CTRL during JJA (not shown).

4.3 Water hosing simulations

We compare our results for IROAM with those from actual water hosing experiments. In the water hosing experiments (see Stouffer et al. 2006 for a detailed description) a freshwater flux of 1 Sv is applied to the North Atlantic for a period of 100 years. The magnitude of the forcing is meant to be representative of actual fluxes occurring during Heinrich events. A total of 9 coupled atmosphere-ocean GCMs participated of which 4 are examined here. These models are the GFDL CM 2.1 (Stouffer et al. 2006), the UKMO HadCM 3 (Hewitt et al. 2006), the University of Toronto GCM (UToronto hereafter; Peltier et al. 2006), and the NCAR CCSM 2.0 (Hu et al. 2008). We calculate moisture transport in these models for the last 20 years of the 100-year forcing period. Figure 10 shows vertical transport profiles. As in the NAC experiment with IROAM, there is a positive contribution from the increased cross-isthmus wind speed in all four water hosing experiments. In difference to IROAM, however, this positive contribution is much weaker and typically confined to the lower troposphere. The contribution from the decreased moisture content is negative throughout the troposphere (except in UToronto) and therefore the overall moisture transport decreases in three out of four models (see Table 3). The only model, in which water hosing increases the cross-American moisture transport is the HadCM 3. In the GFDL CM 2.1 transport changes are slightly negative, and in the UToronto and NCAR CCSM 2.0 simulations there is a pronounced decrease. Thus the wind speed effect in the water hosing experiments is of the same sign as in IROAM but only mitigates the moisture effect rather than reversing it. A possible reason for this is the difference in Atlantic SST patterns (see, e.g., Fig 4 in Timmermann et al 2007). We will discuss this further in section 6. We have also compared the P-E response in the GFDL CM 2.1 with that of IROAM. Qualitatively, the water hosing experiment agrees with IROAM but features a more pronounced negative anomaly that extends further west (not shown).

5 Response to GHG forcing

Under the A1B scenario of GHG increase, temperatures in the tropical oceans increase by about 2-3 K in the AR4 models. The magnitude of SST anomalies is thus comparable to Heinrich events but their sign is opposite. More importantly, the two forcing scenarios differ fundamentally in terms of their spatial distribution because Heinrich events represent a forcing that is confined to the North Atlantic, whereas GHG forcing acts on the entire atmosphere. This is reflected in the simulations examined here as SST and atmospheric moisture changes are centered on the North Atlantic in NAC but spread over the entire globe in the A1B simulations (not shown). There is a moderate increase in cross-isthmus wind speed under CO_2 doubling, possibly because of small differences between Atlantic and Pacific SST warming. This results in an increase in moisture transport across the isthmus, as documented by the positive u'•qm term in Fig. 13. The contribution from the moisture increase (um•q'), however, is about three times larger than u'•qm. This dominance of the moisture increase contrasts with the North Atlantic cooling experiment where the strengthening of the cross-isthmus winds, forced by the localized cooling, was the driving force for the increase in moisture export.

In the ensemble mean, moisture export across the tropical Americas increases by about 29% under global warming (Table 2). This is more than double the 13% increase under North Atlantic cooling (section 4), partly because under global warming both moisture and wind speed changes conspire to increase transport across Central America. The absolute increase is 0.16 Sv, on average, which exceeds the 0.14 Sv standard deviation of transport in the climate of the 20th century (20c3m) simulations and passes the Student's t-test at the 99% level. The substantial increase in Atlantic moisture export should act to strengthen the thermohaline circulation, and thus counteract a potential shutdown. This is discussed in the following section.

When determining the freshwater balance of the Atlantic basin, one must consider, of course, not only transport across America but export from the entire Atlantic drainage basin (see e.g. Zaucker and Broecker 1992 for a definition of the Atlantic drainage basin). Repeating our calculations for this domain we find an ensemble mean export increase of 0.15 Sv under greenhouse gas forcing. This is almost the same as for the export across America only, which indicates that other changes largely cancel each other out. Thus changes in the freshwater balance of the Atlantic basin appear to be dominated by those in cross-American transport.

6 Summary and discussion

We have investigated changes of moisture transport across the tropical Americas in two climate scenarios, Heinrich events and increased GHG forcing. The response of moisture transport to such forcing is important, because it constitutes a strong feedback on the thermohaline circulation via Atlantic salinity changes.

The first part of this study uses a regional coupled ocean-atmosphere model to investigate the impact of Heinrich events by prescribing cold SST anomalies in the North Atlantic. These SST anomalies cool the overlying atmosphere, which leads to two competing effects. On the one hand, the inter-basin pressure gradient increases, leading to an intensification of the northeast trade winds. On the other hand, atmospheric moisture content decreases because of the cooler temperatures and suppressed convection. Of these two effects the trade wind intensification is dominant so that moisture export increases by 0.07 Sv or 13%. For the subtropical North Atlantic this would imply an increase of salinity, which is conducive to deep water formation and strengthening of the AMOC. The increased moisture export would therefore act to restore the AMOC after it has been weakened by an anomalous fresh water flux in the North Atlantic. The estimated freshwater forcing during Heinrich events is on the order of 1.0 Sv. The increased atmospheric moisture flux would therefore offset only 7% of the forcing, but this might become significant under certain conditions.

In addition to the IROAM experiment we also analyzed output from water hosing experiments with four different GCMs. The wind speed contribution to cross-isthmus moisture transport is of the same sign but significantly weaker than in the IROAM North Atlantic cooling experiment. In one of the models, the UKMO HadCM 3, the wind speed effect is still strong enough to produce an overall increase in transport. We note that the hosing experiment of Lohmann (2003) also supports our results with IROAM.

The discrepancy between the IROAM and the water hosing simulations might be due to the difference in their Atlantic SST patterns. The SST anomaly field in the GFDL model, for example, features a zonally oriented tongue of relatively weak cooling around 30°N off the American coast. This could give rise to atmospheric pressure anomalies that induce westerly wind anomalies to the south and weaken the trade winds over northern Central America. Consistently, the GFDL model features decreased cross-isthmus wind speed over northern Central America, and increased winds to the south (not shown).

Thus it remains an open question whether cross-isthmus transport will increase or decrease under freshwater forcing. We have shown, however, that the change in cross-isthmus moisture transport is the residual of two large, opposing effects from the intensified trades and reduced moisture. Due to the cancellation of these two terms the actual change in moisture transport is likely to be small.

Precipitation decreases on both sides of the isthmus in response to the cold North Atlantic SST anomalies. This is the case for both IROAM and the water hosing simulations. In IROAM, it is due to two factors: 1) The cold SST anomalies suppress convection locally in the Caribbean and remotely in the eastern Pacific through subsidence Rossby waves and cold temperature advection. 2) The intensified cross-isthmus winds, through their effect on sensible and latent heat fluxes, cool SSTs in the far eastern Pacific and thus shift major precipitation southward and westward. As a result of the precipitation changes, North Atlantic cooling acts to increase salinity in the far eastern Pacific despite the increased moisture flux from the Atlantic side. The response of salinity in coastal regions might be complicated further by the intensification of the gap winds and attendant changes in windstress curl and upwelling. Since the gap winds induce negative windstress curl and upwelling on their southern flank, their intensification leads to increased upwelling in those areas. This should increase salinity as high salinity water is brought to the surface. In IROAM surface salinity is restored to climatology so that we cannot estimate the strength of this effect. We note, however, that the water hosing experiments feature increased sea surface salinity when a 0.1 Sv freshwater flux is applied (Stouffer et al. 2006, their figure 9b).

The above discussion shows that circulation changes associated with North Atlantic cooling can lead to a complex, non-uniform precipitation response in the eastern Pacific. This suggests that great caution should be exercised in the interpretation of proxy records from the region. Furthermore, results from one particular measurement site might not be representative of the entire region.

The response of moisture export to North Atlantic cooling is highly seasonal, with a strong increase between May and December, and a slight decrease between January and April. This seasonality is to be expected because in the summertime the cold SST anomaly inhibits ITCZ precipitation and the associated low-level moisture convergence.

In the second part of this study we use IPCC AR4 output as well as reanalysis data to estimate transport under present day conditions. Both IROAM and AR4 models tend to simulate stronger transport across the tropical Americas than do the reanalyses. There is, however, no clear indication of a resolution dependence.

In the third part, we use the A1B simulations to calculate the response of moisture transport under global warming. In these simulations, the ubiquitous increase of atmospheric moisture leads to an increase in transport across the tropical Americas by about 0.16 Sv in the ensemble mean. This result remains almost unchanged if the entire Atlantic drainage basin is considered. In comparison, Stouffer et al. (2006) estimate that, under CO_2 quadrupling, changes in precipitation, river run-off and glacier melting could lead to a North Atlantic fresh water flux of about 0.2 Sv. Considering that the 0.16 Sv in this study were obtained for the a1b scenario (in which CO_2 roughly doubles) it seems likely that the increase in atmospheric moisture transport could offset much of the warming-induced freshwater flux in the North Atlantic.

In relative terms, the atmospheric moisture transport in the a1b experiments increases by about 25%, which is significantly higher than the 13% obtained in the North Atlantic cooling experiment of the first part. This is due to the fact that in the global warming case both wind speed and moisture changes conspire to increase transport, whereas these influences oppose each other in the North Atlantic cooling experiment.

We note several caveats concerning this study. First, Atlantic SSTs are prescribed in the IROAM North Atlantic cooling experiment, and might differ significantly from actual fresh water flux scenarios. Second, the lateral boundary conditions in IROAM are the same between the control and North Atlantic cooling experiments. This might constrain the behavior of the anomaly experiment to some extent but our experience with the regional model suggests that this influence is small. Third, changes in the global thermohaline circulation cannot be captured in the regional model, and thus the SST response in the Pacific might differ from that of multi-century GCM water hosing experiments. This might affect the inter-basin pressure gradient as well as P-E fluxes over the Pacific. We note, however, that the P-E changes in IROAM are qualitatively similar to those in the GFDL water hosing experiment.

Moisture transport across the Andes accounts for roughly half of the total transport in all the models and the JRA-25 reanalysis. This holds true regardless of model resolution, which varies from 0.5° in IROAM to about 5° in some of the GCMs. If these results are realistic, then the often invoked blocking effect of the Andes might not play any significant role in terms of moisture transport. However, there is certainly reason to doubt that even 0.5° resolution is adequate to resolve the relevant orographic features of the Andes. It is therefore entirely possible that current climate models cannot properly simulate the blocking effect of the Andes. This might lead them to misrepresent an important aspect of the response of the climate system to North Atlantic cooling. Further efforts with high resolution models are needed to shed more light on the potential role of the Andes as a moisture barrier.

Acknowledgments

This study was supported by the NOAA Climate Program Office, and the Japan Agency for Marine-Earth Science and Technology (JAMSTEC) through its sponsorship of the International Pacific Research Center. The authors are grateful to the following individuals for generously providing us with their water hosing data: Ronald Stouffer and Jianjun Yin (GFDL CM 2.1), Aixue Hu (NCAR CCSM 2.0), Jonathan Gregory and Kevin Marsh (UKMO HadCM 3), and Guido Vettoretti (UToronto). The authors wish to thank Justin Small for help in the moisture transport calculations and valuable comments on the manuscript. Thanks also to the three anonymous reviewers for their helpful suggestions. IPRC/SOEST publication #660/7857.

References

Benway HM, Mix AC, Haley BA, Klinkhammer GP (2006) Eastern Pacific Warm Pool paleosalinity and climate variability: 0-30 kyr. Paleoceanography 21, doi:10.1029/2005PA001208.

Broecker WS (1997) Thermohaline circulation, the Achilles heel of our climate system: will man-made CO_2 upset the current balance? Science 278: 1582-1588

Broecker WS (2003) Does the trigger for abrupt climate change reside in the ocean or in the atmosphere? Science 300: 1519-1522

Chan WL, Motoi T (2005) Response of thermohaline circulation and thermal structure to removal of ice sheets and high atmospheric CO_2 concentration. Geophys Res Lett 32: L07601

Clark PU, Pisias N, Stocker TF, Weaver AJ (2002) The role of the thermohaline circulation in abrupt climate change. Nature 415: 863-869

Dickinson RE, Henderson-Sellers A, Kennedy PJ (1993) Biosphere-Atmosphere Transfer Scheme (BASTS) version 1e as coupled to the NCAR Community Climate Model. NCAR Tech Note NCAR/TN-387+STR, 72pp

Edwards JM, Slingo A (1996) Studies with a flexible new radiation code I: Choosing a configuration for a large-scale model. Quart J Roy Meteor Soc 122: 689-719

Gregory JM, and co-authors (2005) A model intercomparison of changes in the Atlantic thermohaline circulation in response to increasing atmospheric CO2 concentration Geophys Res Lett 32: L12703, doi:10.1029/2005GL023209

Hemming SR (2004) Heinrich events: massive late Pleistocene detritus layers of the North Atlantic and their global climate imprint. Rev Geophys 42: RG1005, doi:10.1029/2003RG000128.

Hewitt CD, Broccoli AJ, Crucifix M, Gregory JM, Mitchell JFB, Stouffer RJ (2006) The effect of a large freshwater perturbation on the glacial North Atlantic Ocean using a coupled general circulation model. J Climate 19: 4436–4447

Hu A, Otto-Bliesner BL, Meehl GA, Han W, Morrill C, Brady EC, Briegleb B (2008) Response of thermohaline circulation to freshwater forcing under present-day and LGM conditions. J Climate 21: 2239–2258

Kalnay E, and co-authors (1996) The NCEP/NCAR 40-Year Reanalysis Project. Bull Amer Meteor Soc 77: 437–471

Langland RH, Liou CS (1996) Implementation of an E-ε parameterization of vertical subgrid-scale mixing in a regional model. Mon Wea Rev 124: 905-918

Latif M, Roeckner E, Mikolajewicz U, Voss R (2000) Tropical stabilization of the thermohaline circulation in a greenhouse warming simulation. J Climate 13: 1809-1813

Leduc G, Vidal L, Tachikawa K, Rostek F, Sonzogni C, Beaufort L, Bard E (2007), Moisture transport across Central America as a positive feedback on abrupt climatic changes. Nature 445: 908-911

Levitus S (1982) *Climatological Atlas of the World Ocean*. NOAA Prof. Paper No. 13, 173 pp. and 17 microfiche.

Lohmann G, Lorenz S (2000) On the hydrological cycle under paleoclimatic conditions as derived from AGCM simulations. J Geophys Res 105: 17,417-17,436

Lohmann G (2003) Atmospheric and oceanic freshwater transport during weak Atlantic overturning circulation. Tellus 55A: 438-449

Manabe S, Stouffer RJ (1988) Two stable equilibria of a coupled ocean-atmosphere model. J Climate 1: 841-866

Manabe S, Stouffer R (1994) Multiple-century response of a coupled ocean–atmosphere model to an increase of atmospheric carbon dioxide. J Climate 7: 5–23

Onogi K, and co-authors, (2007), The JRA-25 Reanalysis, *J. Meteorol. Soc. Japan*, *85*, 369-432

Pacanowski RC (1996) Documentation user's guide and reference manual of MOM2, Version 2. GFDL Ocean Tech. Rep. 3.2, Princeton, NJ, 329 pp.

Pahnke K, Sachs J, Keigwin L, Timmermann A, Xie S-P (2007) Eastern tropical Pacific hydrologic changes during the past 27,000 years from D/H ratios in alkenones. Paleoceanography 22: doi:10.1029/2007PA001468.

Peltier WR, Vettoretti G, Stastna M (2006) Atlantic meridional overturning and climate response to Arctic Ocean freshening. Geophys Res Lett 33: L06713, doi:10.1029/2005GL025251

Romanova V, Prange M, Lohmann G (2004) Stability of the glacial thermohaline circulation and its dependence on the background hydrological cycle. Clim Dyn 22: 527-538

Schiller A, Mikolajewicz U, Voss R (1997) The stability of the thermohaline circulation in a coupled ocean-atmosphere model. Climate Dyn 13: 325-348

Stouffer R, Manabe S (1999) Response of a coupled ocean-atmosphere model to increasing atmospheric carbon dioxide: sensitivity to the rate of increase. J Climate 12: 2224-2237

Stouffer R, and co-authors (2006) Investigating the causes of the response of the thermohaline circulation to past and future climate changes. J Climate 19:1365–1387

Sun Z, Rilkus L (1999) Improved application of exponential sum fitting to inhomogeneous atmosphere. J Geophys Res 104: 6291-6303

Swingedouw D, Braconnot P, Delecluse P, Guilyardi E, Marti O (2007) Quantifying the AMOC feedbacks during a 2xCO2 stabilization experiment with land-ice melting, Climate Dyn 29: 521-534.

Tiedtke M (1989) A comprehensive mass flux scheme for cumulus parameterization in large-scale models. Mon Wea Rev 117**:** 1779–1800

Timmermann A, Okumura Y, An SI, Clement A, Dong B, Guilyardi E, Hu A, Jungclaus JH, Renold M, Stocker TF, Stouffer RJ, Sutton R, Xie SP, Yin J (2007) The Influence of a Weakening of the Atlantic Meridional Overturning Circulation on ENSO. J. Climate 20: 4899–4919

Uppala SM, and co-authors (2005) The ERA-40 re-analysis. Quart J Roy Meteor Soc 131: 2961–3012

Wang Y (2001) An explicit simulation of tropical cyclones with a triply nested movable mesh primitive equation model: TCM3. Part I: Model description and control experiment. Mon Wea Rev 129: 1370-1394

Wang Y, Sen OL, Wang B (2003) A highly resolved regional climate model (IPRC-RegCM) and its simulation of the 1998 severe precipitation events over China. Part I: Model description and verification of simulation. J Climate 16: 1721–1738

Wang Y, Xie S-P, Xu H, Wang B (2004) Regional Model Simulations of Marine Boundary Layer Clouds over the Southeast Pacific off South America. Part I: Control Experiment. Mon Wea Rev 132: 274–296

Xie S-P, Okumura Y, Miyama T, Timmermann A (2008) Influences of Atlantic climate change on the tropical Pacific through the Central American isthmus. J Climate 21: 3914-3928

Xie S-P, Miyama T, Wang Y, Xu H, de Szoeke SP, Small RJ, Richards KJ, Mochizuki T, and Awaji T (2007) A regional ocean-atmosphere model for eastern Pacific climate: Towards reducing tropical biases. J Climate 20: 1504–1522

Xie S-P, Xu H, Kessler WS, Nonaka M (2005) Air-sea interaction over the eastern Pacific warm pool: Gap winds, thermocline dome, and atmospheric convection. J Climate 18: 5-25

Xu H, Xie S-P, Wang Y, Small RJ (2005) Effects of Central American mountains on the eastern Pacific winter ITCZ and moisture transport. J Climate 18: 3856–3873

Zaucker F, Broecker WS (1992) The influence of atmospheric moisture transport on the fresh water balance of the Atlantic drainage basin: general circulation model simulations and observations. J Geophys Res 97: 2765-2773

Zheng Y, van Geen A, Anderson RF, Gardner JV, Dean WE (2000) Intensification of the northeast Pacific oxygen minimum zone during the Bölling-Alleröd warm period. Paleoceanography 15: 528-536

Zhou T, Zhang X, Wang S (2000) The interbasin transport of atmospheric moisture evaluated from NCEP/NCAR reanalysis data. Acta Meteor Sin 14: 159-172

Tables

Model	Modeling Center
BCCR BCM 2.0	Bjerknes Centre for Climate Research, Norway
CNRM CM 3	Centre National de Recherches Meterologiques, France
CSIRO Mk 3.5	Commonwealth Scientific and Industrial Research Organization, Australia
GFDL CM 2.0	Geophysical Fluid Dynamics Laboratory, USA
GFDL CM 2.1	Geophysical Fluid Dynamics Laboratory, USA
GISS AOM	NASA / Goddard Institute for Space Studies, USA
GISS Model EH	NASA / Goddard Institute for Space Studies, USA
GISS Model ER	NASA / Goddard Institute for Space Studies, USA
IAP FGOALS g1.0	LASG / Institute of Atmospheric Physics, China
INGV ECHAM4	Instituto Nazionale di Geofisica e Vulcanologia, Italy
INMCM 3.0	Institute for Numerical Mathematics, Russia
IPSL CM 4	Institut Pierre-Simon Laplace, France
MIROC 3.2 (high resolution)	Center for Climate System Research (CCSR), Japan
MIROC 3.2 (low resolution)	Center for Climate System Research (CCSR), Japan
MPI ECHAM 5	Max Planck Institute for Meteorology, Germany
NCAR CCSM 3.0	National Center for Atmospheric Research, USA
NCAR PCM 1	National Center for Atmospheric Research, USA
UKMO HadGEM 1	Met Office Hadley Centre for Climate Prediction, UK

Table 1. The IPCC AR4 models used in this study.

Model	horizontal resolution	transport across subtrop Am [Sv] (20c3m)	increase of transport under GHG forcing [Sv]
ERA 40	0.8x0.8 (T159)	0.340	N/A
JRA 25	1.1x1.1 (T106)	0.404	N/A
NCEP (Zhou et al.)	2.5x2.5	1.05	N/A
IROAM	0.5x0.5	0.539	N/A
observations (Zaucker et al.)		0.36	N/A
AR4 ensemble mean	N/A	0.555	0.163 (29.3%)
BCCR BCM 2.0	2.8x2.8 (T42)	0.324	0.106 (32.6%)
CNRM CM 3	2.8x2.8 (T42)	0.521	0.110 (21.2%)
CSIRO Mk 3.5	1.9x1.9 (T63)	0.720	0.205 (28.4%)
GFDL CM 2.0	2.5x2.0	0.500	0.175 (35.1%)
GFDL CM 2.1	2.5x2.0	0.673	0.202 (30.1%)
GISS AOM	4x3	0.330	0.151 (45.7%)
GISS Model EH	5x4	0.536	0.139 (26.0%)
GISS Model ER	5x4	0.553	0.134 (24.3%)
IAP FGOALS g1.0	2.8x2.8	0.720	0.152 (21.1%)
INGV ECHAM4	1.1x1.1 (T106)	0.495	0.151 (30.4%)
INMCM 3.0	5x4	0.680	0.162 (23.9%)
IPSL CM 4	2.5x3.8	0.672	0.218 (32.5%)
MIROC 3.2 hi-res	1.1x1.1 (T106)	0.514	0.249 (48.5%)
MIROC 3.2 med-res	2.8x2.8 (T42)	0.707	0.235 (33.2%)
MPI ECHAM 5	1.9x1.9 (T63)	0.594	0.231 (39.0%)
NCAR CCSM 3.0	1.4x1.4 (T85)	0.672	0.124 (18.5%)
NCAR PCM 1	2.8x2.8 (T42)	0.490	0.079 (16.2%)
UKMO HadGem 1	1.9x1.3	0.290	0.104 (35.9%)

Table 2. Moisture transport [Sv] across subtropical America (segments 5-12 in Fig. 1) under present day conditions (column 3) and its increase under global warming (column 4). Listed are the ERA 40 and JRA 25 reanalyses, IROAM, and the IPCC AR4 models. Also shown are results of other authors for NCEP Reanalysis (*Zhou et al.*, 2000) and observations (*Zaucker and Broecker*, 1992). The horizontal resolution for models and reanalyses are shown in the second column.

Model	transport across subtrop Am [Sv] control run	transport across subtrop Am [Sv] 1Sv hosing run	difference [Sv] hosing - control
GFDL CM 2.1	0.611	0.595	-0.016 (-2.6%)
UKMO HadCM 3	0.458	0.465	+0.007 (+1.5%)
UToronto	0.416	0.328	-0.088 (-21.2%)
NCAR CCSM 2.0	0.777	0.687	-0.090 (-13.1%)

Table 3: Moisture transport [Sv] across subtropical America (segments 5-12 in Fig. 1) for several water hosing experiments (column 2) and their corresponding control simulation (column3). The difference (water hosing – control) is shown in column 4.

Figures

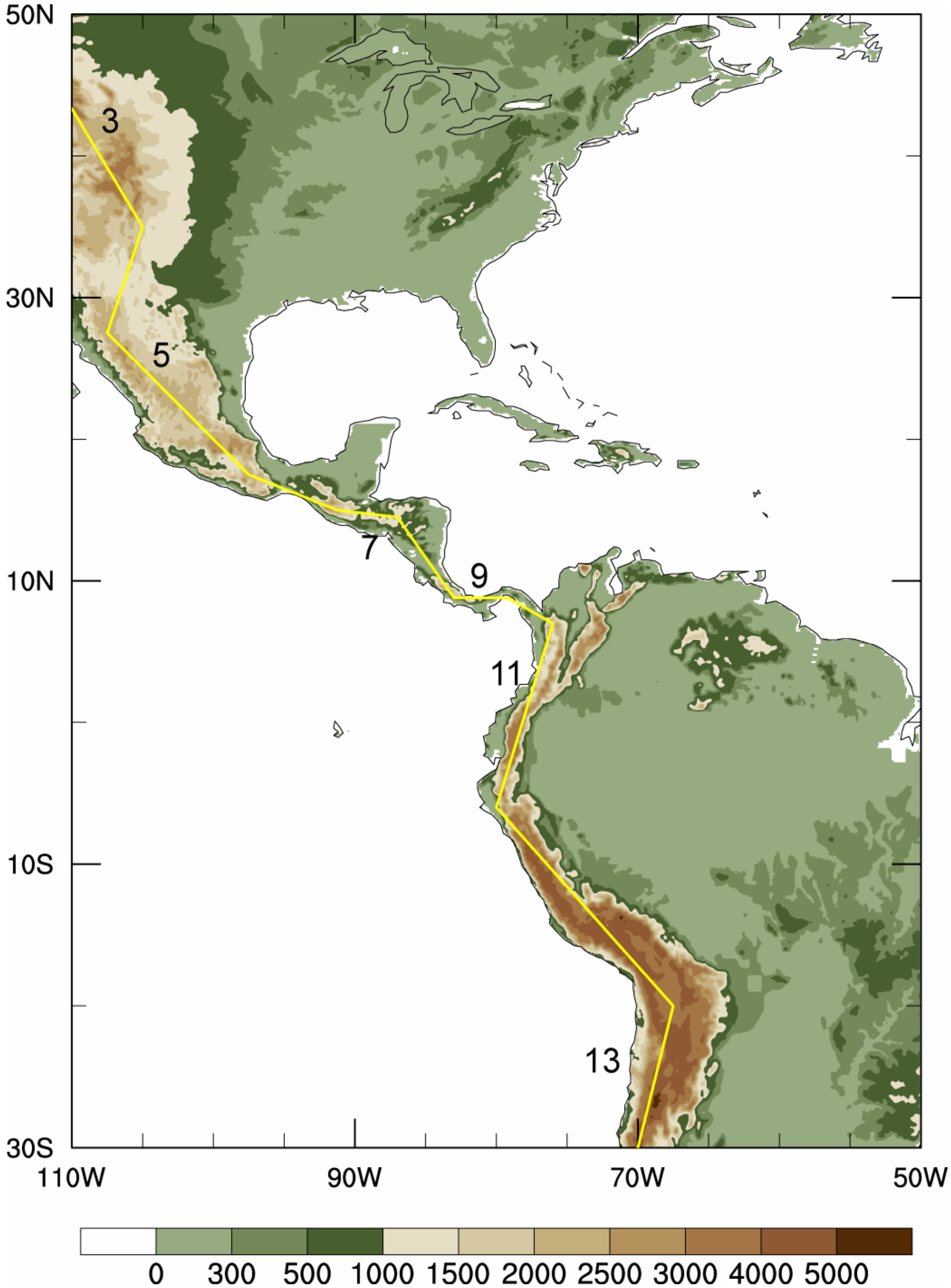

Fig. 1 ETOPO5 orography (m, shading), and the line segments across which moisture transport is calculated (yellow line). Light smoothing has been applied to the orography field.

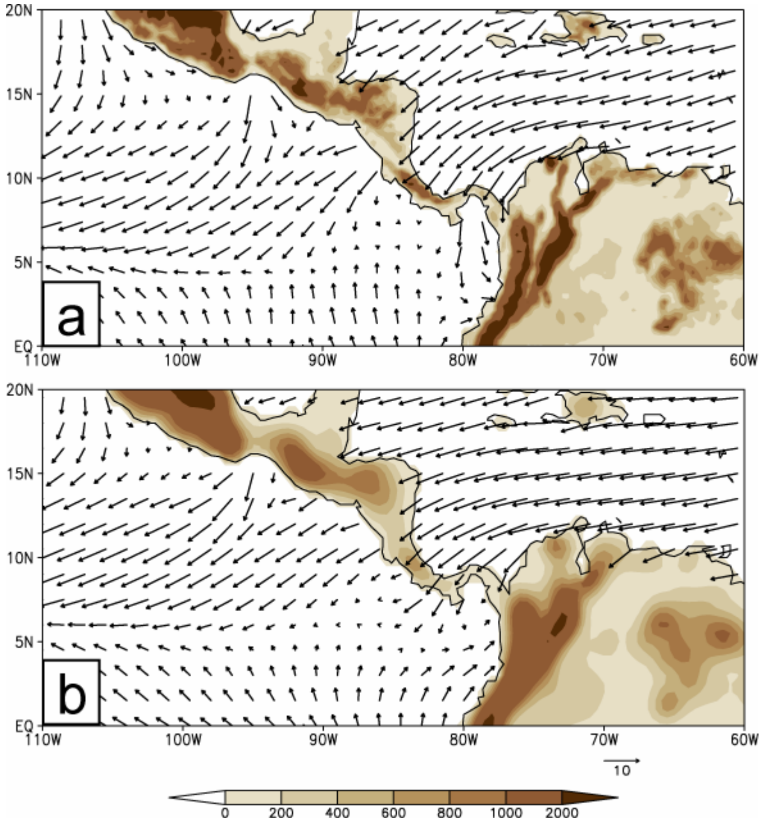

Fig. 2 Orography (m, shading) and Jan-Feb mean winds at 10 m height (m/s, vectors). The individual panels show (a) ETOPO5 orography and QuickSCAT surface winds on a 0.25° by 0.25° grid, and (b) IROAM orography and surface winds on the model's 0.5° by 0.5° grid.

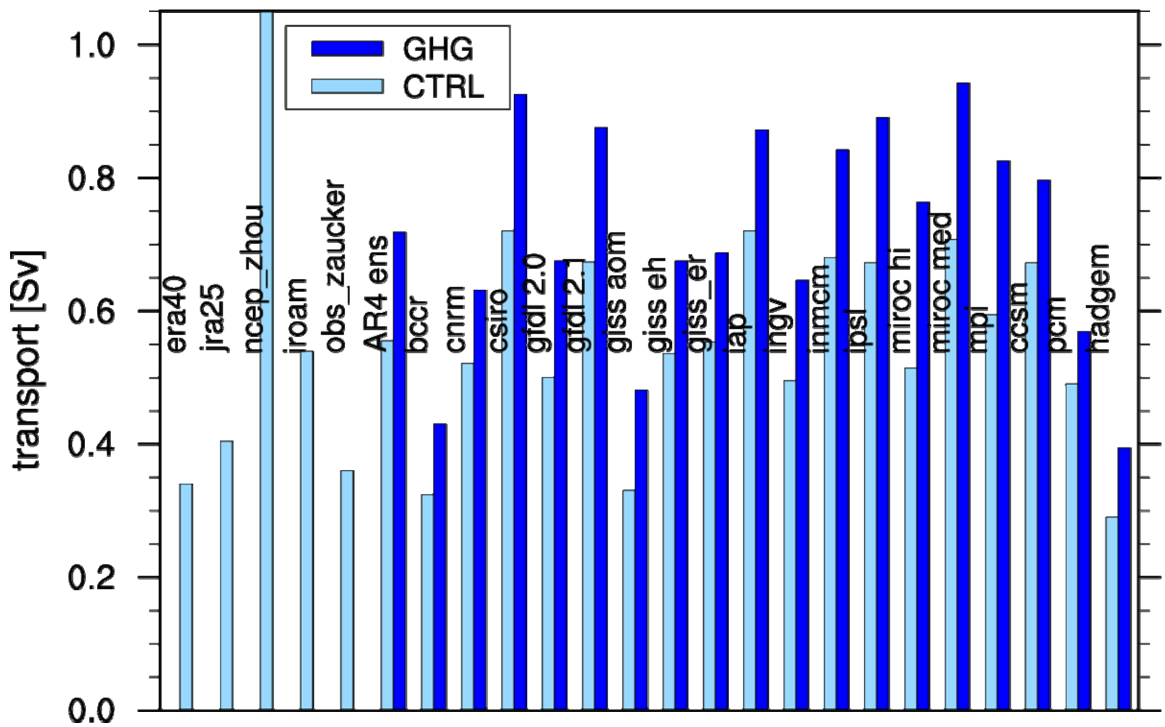

Fig. 3 Bar chart of the transports [Sv] listed in Table 2. The light blue bar indicates observations/control simulations, the dark blue bar global warming simulations.

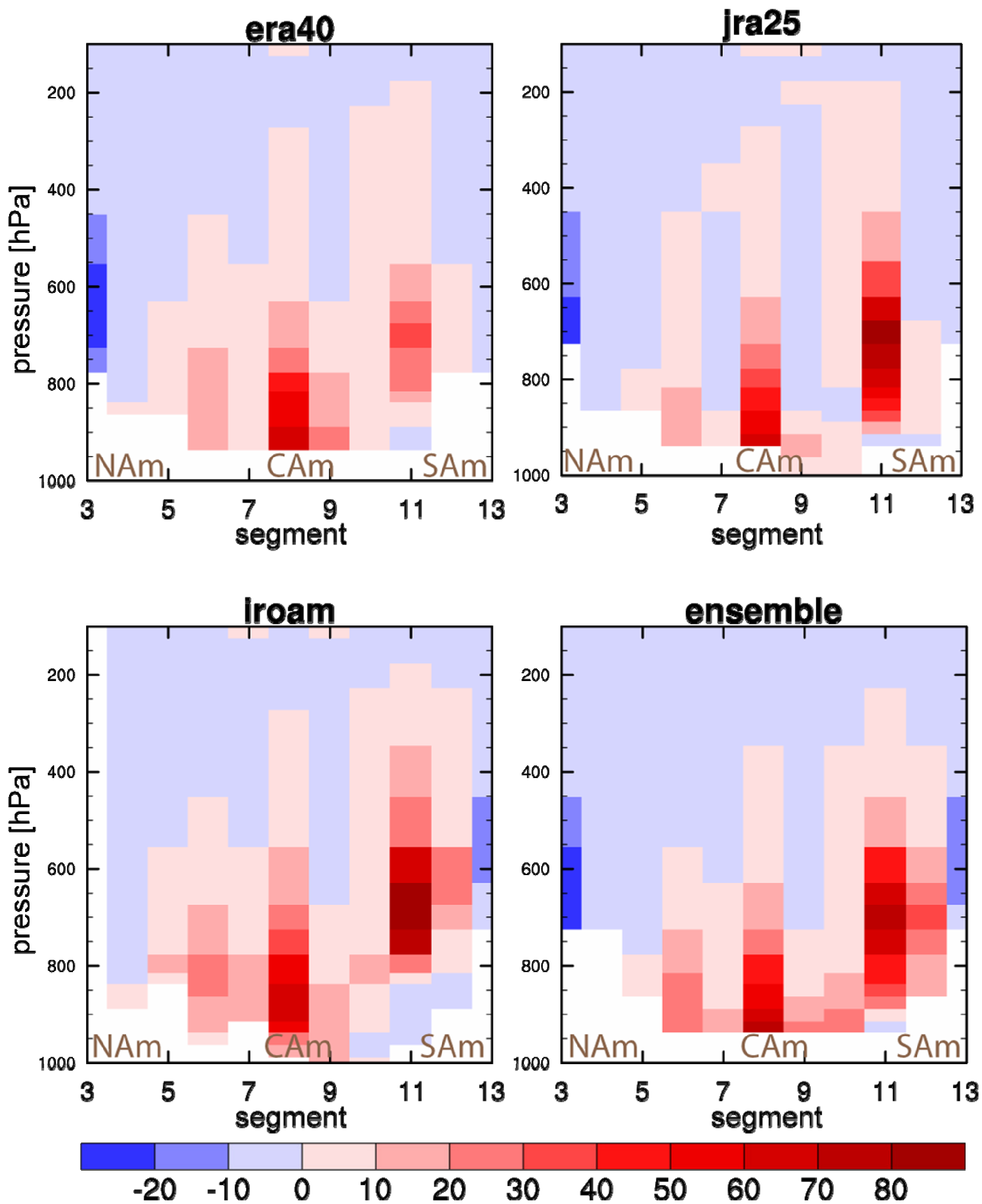

Fig. 4 Height-segment sections of moisture flux integrated along segment lines (kg m^2 s^{-1} kg^{-1} E3) for present day conditions. Segment numbers correspond to Fig. 1. The individual panels show results for the ERA 40 and JRA 25 reanalyses, IROAM, and the ensemble mean of IPCC AR4 models listed in Table 1. The white areas indicate the orography. The approximate positions of North, South and Central America are indicated along the horizontal axis.

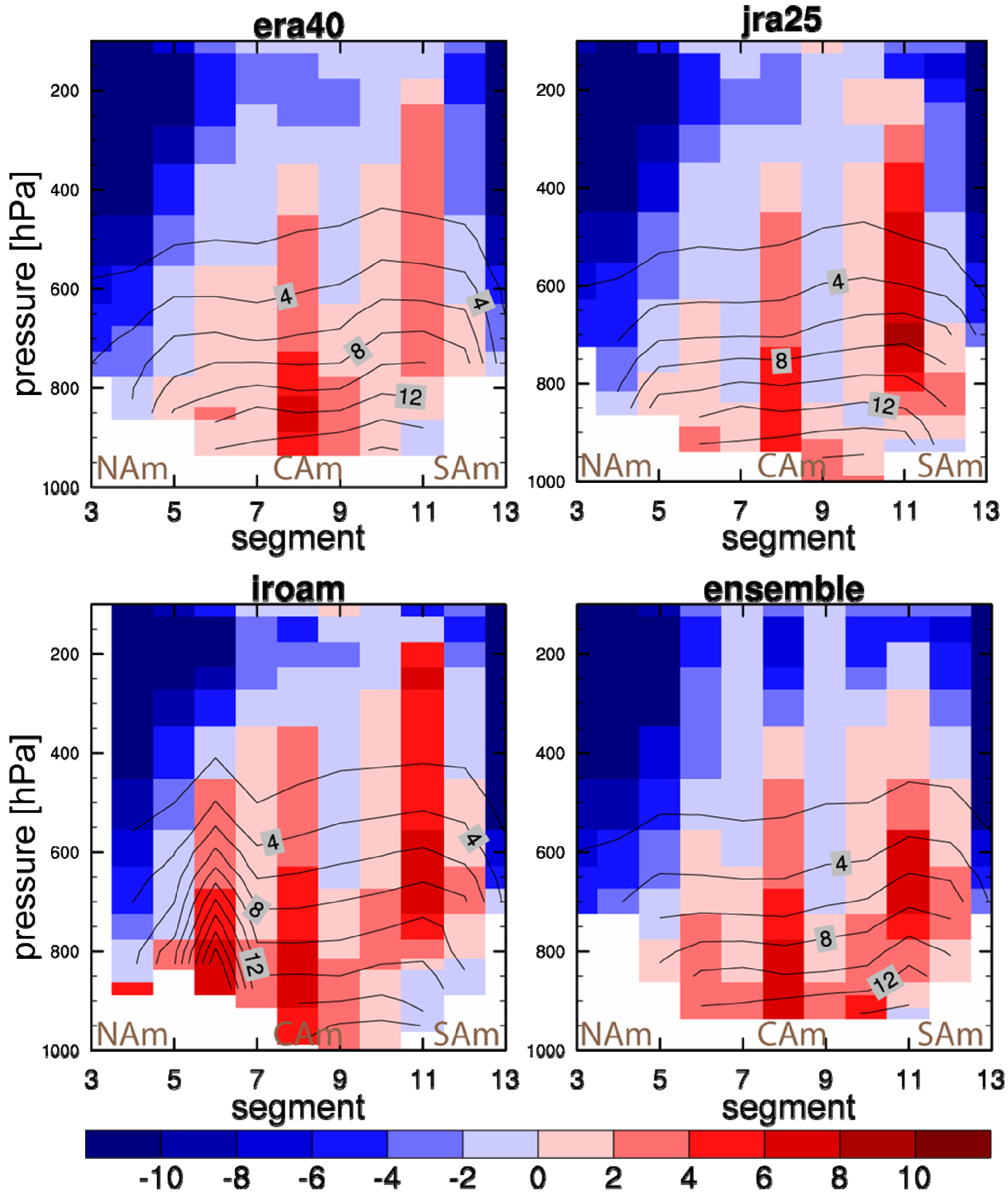

Fig. 5 As in Fig. 4 but for specific humidity (contours; g/kg) and cross-segment wind speed (shading; m/s).

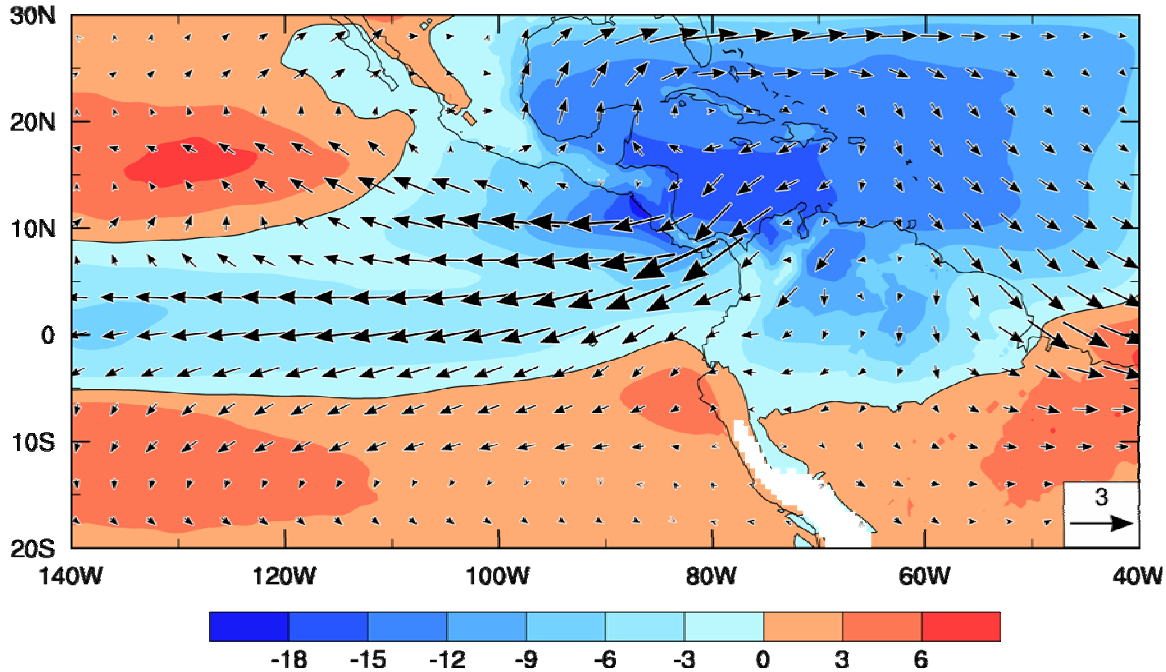

Fig. 6 Difference between NAC and CTRL with respect to average wind (vectors; m/s) and precipitable water (shading; kg m-2) between 1000 and 700 hPa. The zero-line of precipitable water is marked by a black contour. The fields represent the climatological annual mean.

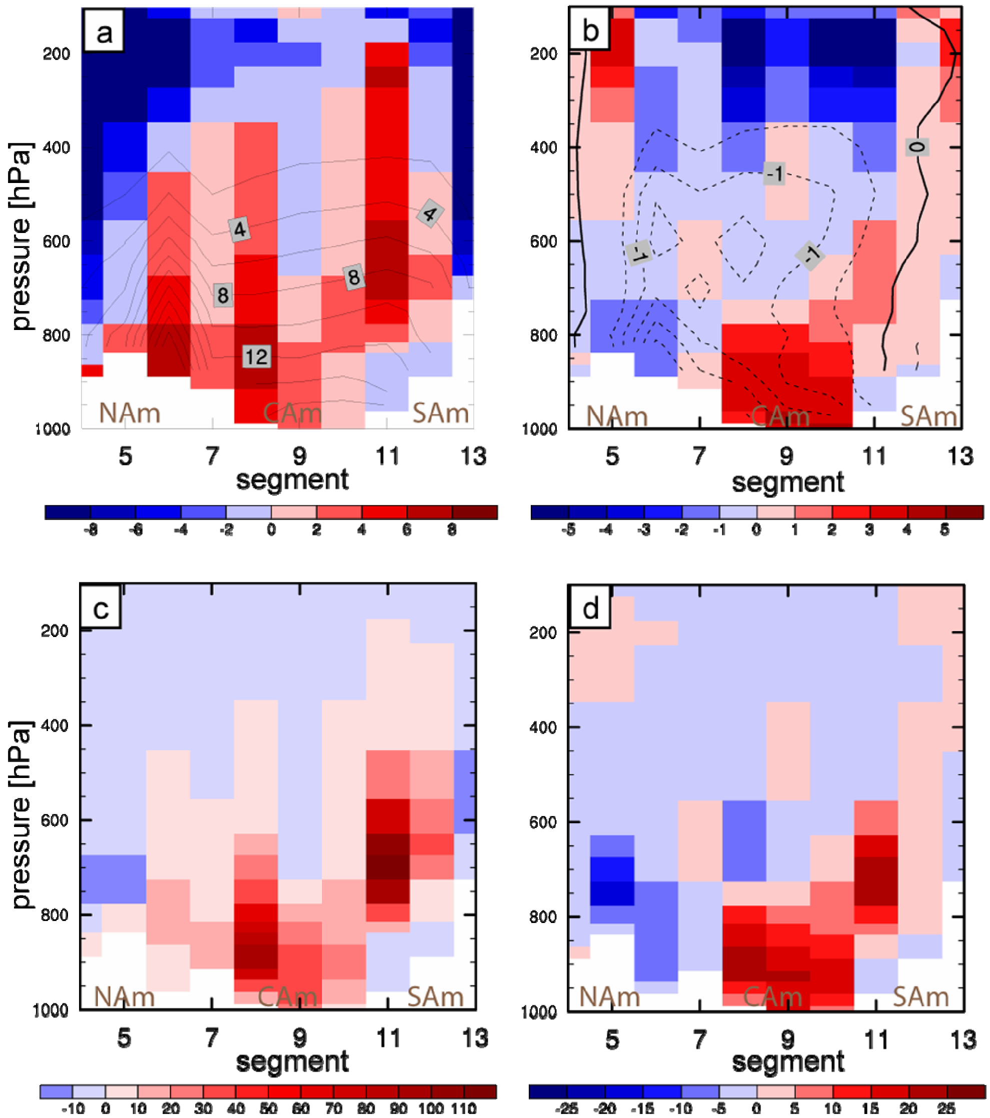

Fig. 7 Upper panels: wind speed (m/s, shading) and specific humidity (g/kg, contours) along the line segments shown in Fig. 1. The wind speed is oriented normal to the line segments with a positive sign indicating flow toward the Pacific basin. Negative humidity contours are dashed. The panels show (a) the control simulation (CTRL), and (b) the difference of the North Atlantic cooling (NAC) and CTRL simulations. The lower panels show moisture flux integrated along segment lines (kg m^2 s^{-1} kg^{-1} E3) for (c) the CTRL simulation, and (d) the difference NAC minus CTRL.

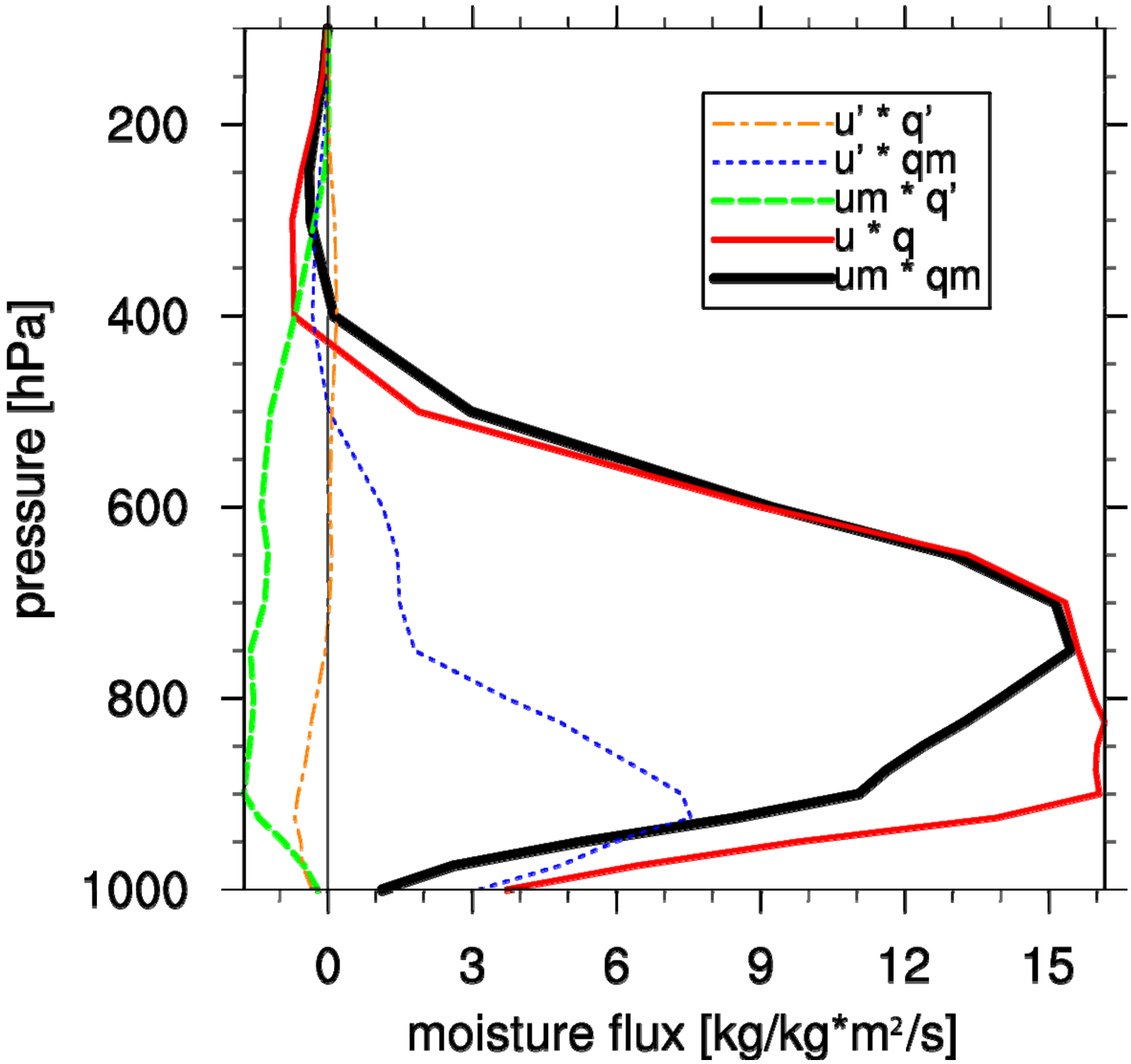

Fig. 8 Vertical profiles of annual mean moisture flux (kg m^2 s-1 kg-1 *E3) integrated along the line segments 5-10 (Central America) in Fig. 1. The flux is decomposed into the following components (see section 2): CTRL (um•qm; thick black line), NAC (u•q; red line), and contributions from change in humidity (um•q'; dashed green line), change in windspeed (u'•qm; dotted blue line), and change in humidity and windspeed (u'•q'; dashed-dotted orange line). The latter three terms add up to the moisture flux difference between CTRL and NAC, i.e. uq - um•qm = um•q' + u'•qm + u'•q'.

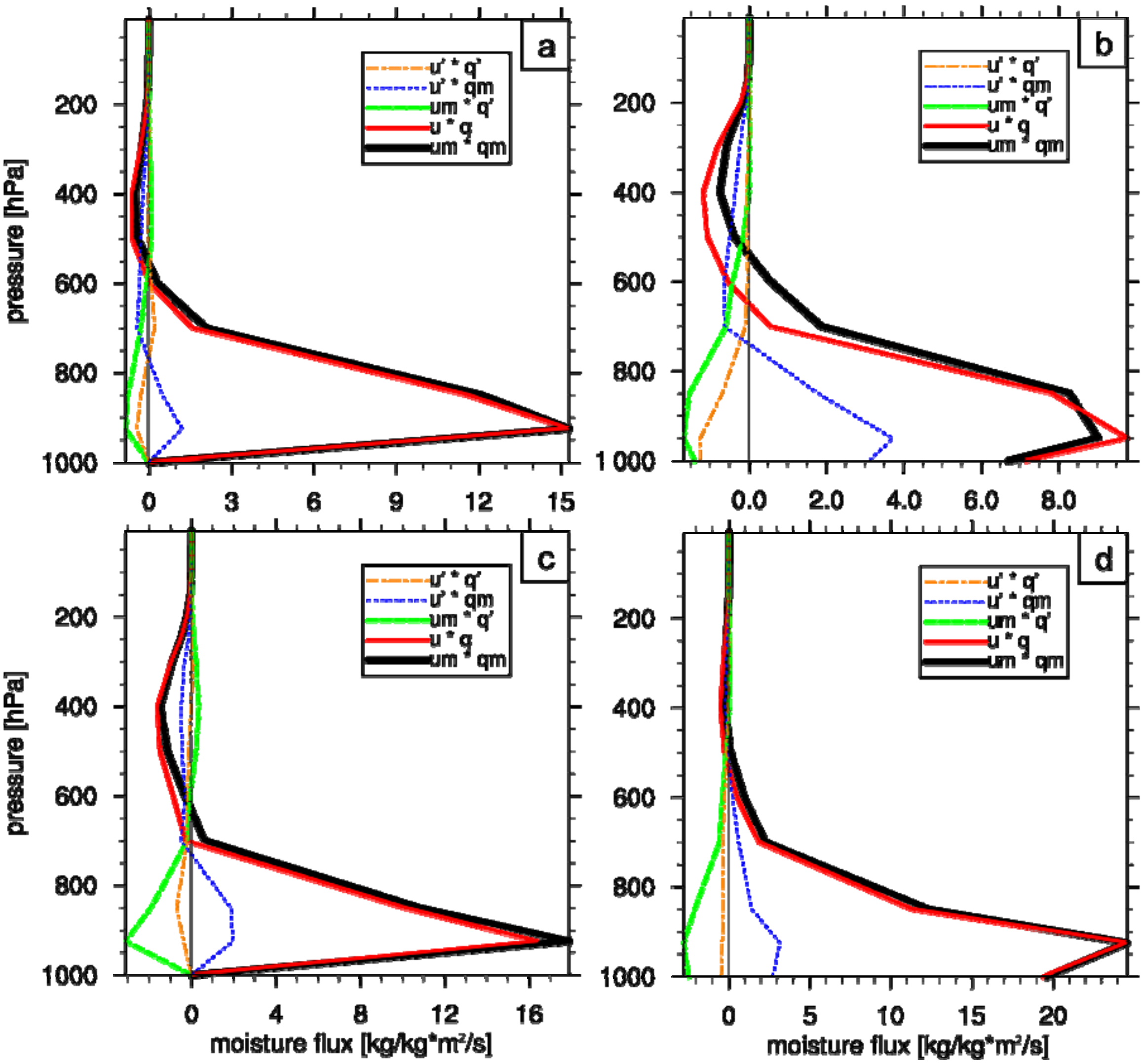

Fig. 9 Same as in Fig. 8 but for the water hosing experiments. The thick black line denotes the control simulation of each model whereas the red line denotes the 1 Sv water hosing simulation. The individual panels show (a) GFDL CM 2.1, (b) UKMO HadCM 3.0, (c) University of Toronto Model, and (d) NCAR CCSM 2.0. Note the different scales for the x-axes.

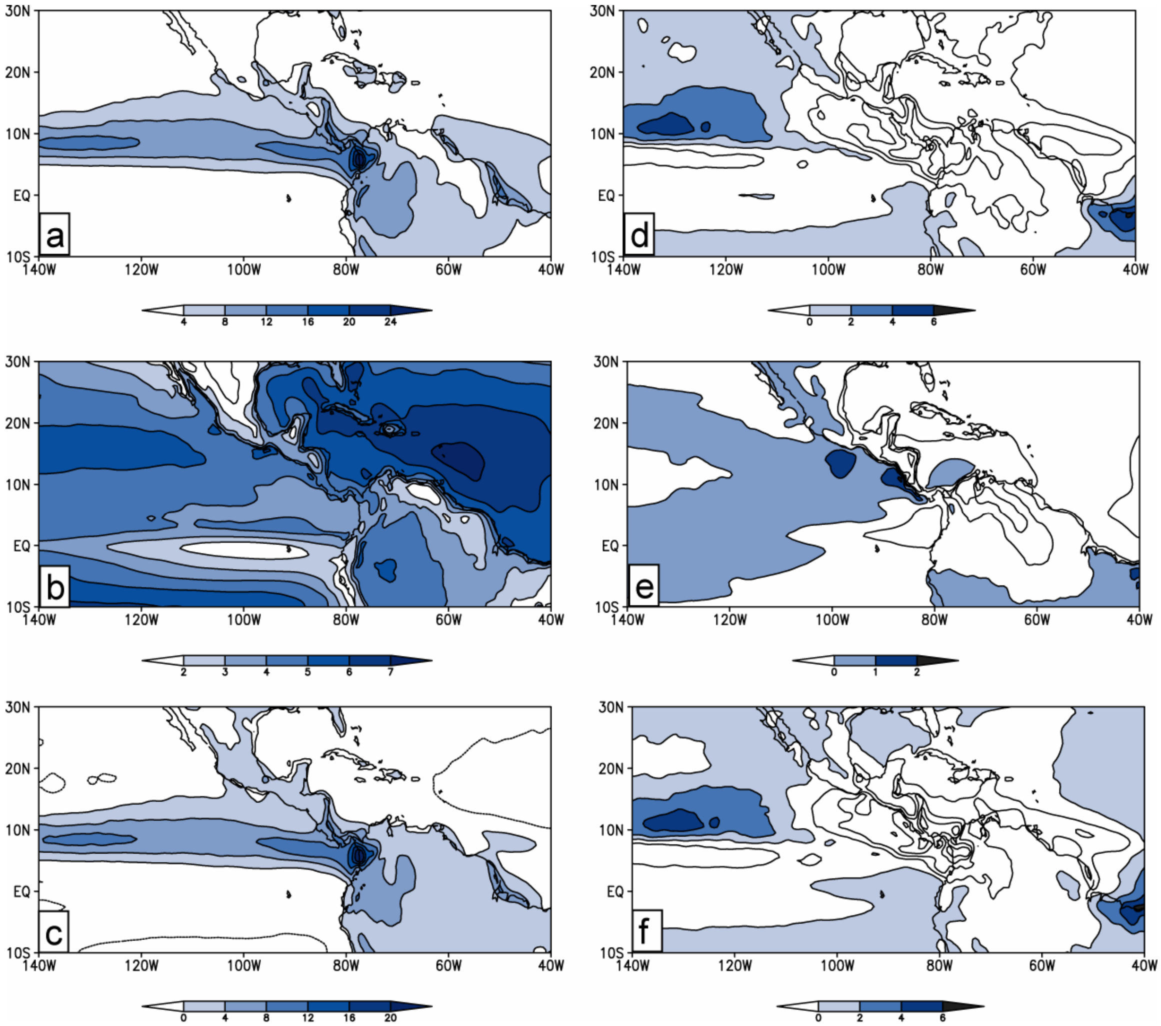

Fig. 10 Annual means of CTRL (left column) and NAC minus CTRL (right column) for the following fields: (a) + (d) precipitation (mm/day), (b) + (e) evaporation (mm/day), and (c) + (f) precipitation minus evaporation (mm/day, P-E). Positive values are shaded.

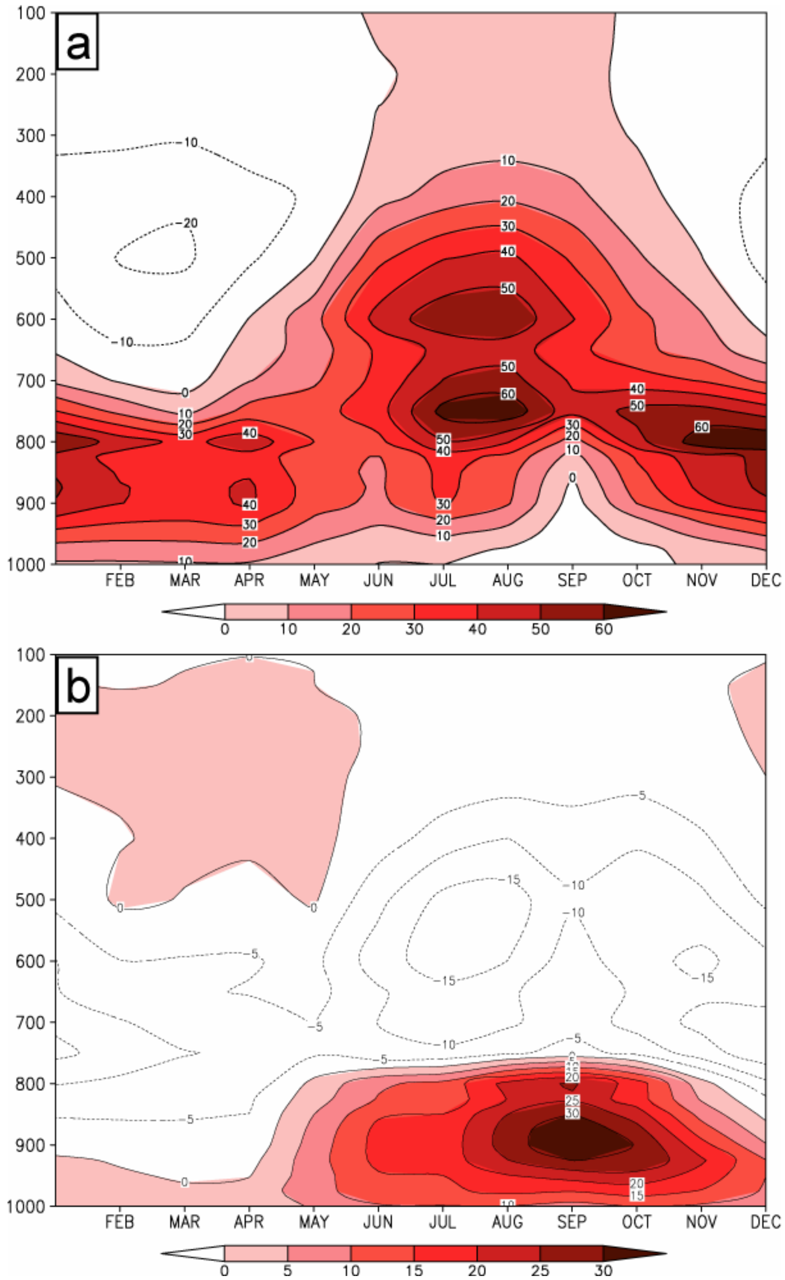

Fig. 11 Height-time sections of moisture transport (kg m^{-3} 10^{3}) across segments 5-10 (Central American isthmus) in Fig. 1 for (a) CTRL, (b) the difference NAC – CTRL. Positive values are shaded.

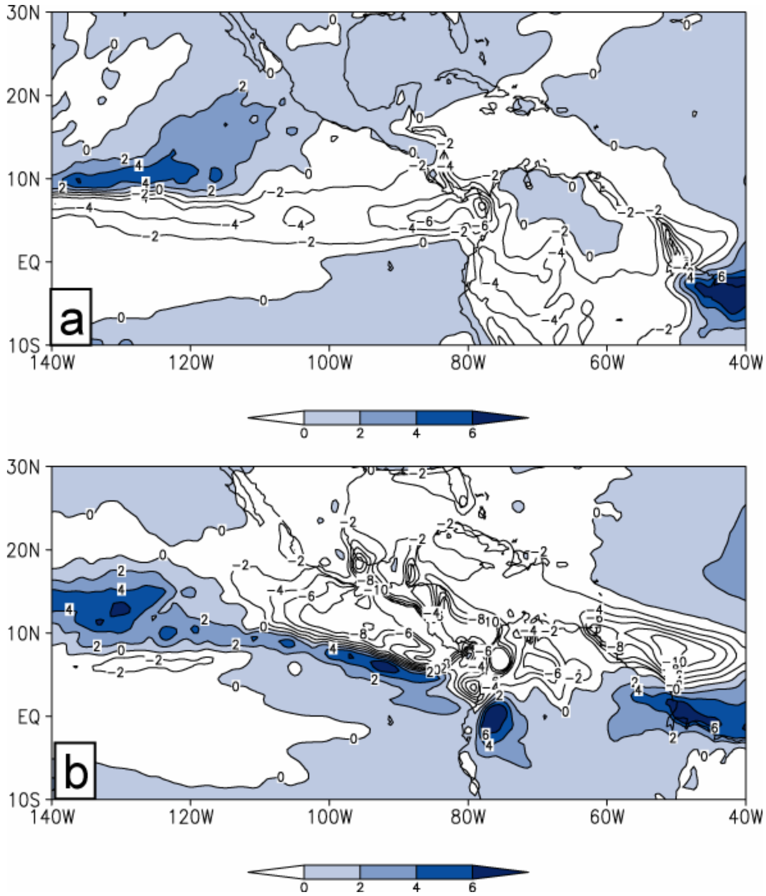

Fig. 12 P-E difference between NAC and CTRL (mm/day) for (a) DJF, and (b) JJA. Positive values are shaded.

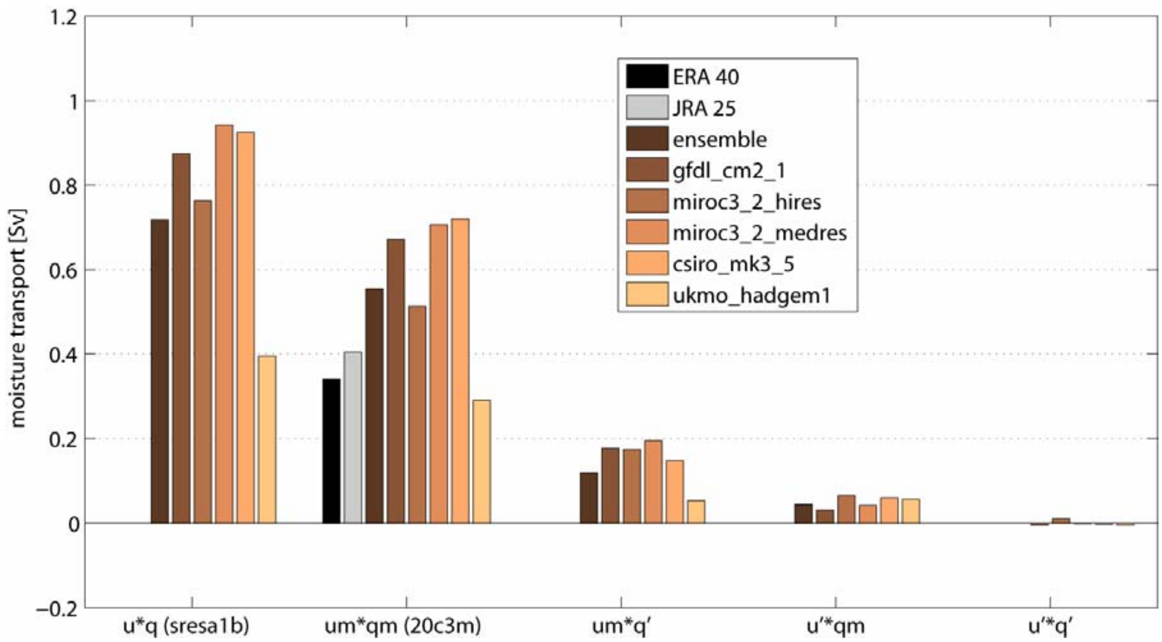

Fig. 13 Moisture transport [Sv] across subtropical America for various models. The individual clusters show, from left to right, the 2080-2100 average for CO2 doubling experiments (sresa1b), the 1980-2000 average for twentieth century experiments (20c3m), and the following three contributions to the difference between sresa1b and 20c3m experiments: moisture perturbation, wind speed perturbation, and the product of moisture and wind speed perturbations.